2014 IEEE Intelligent Vehicles Symposium (IV)
June 8-11, 2014. Dearborn, Michigan, USA

A Novel Method for Extrinsic Parameters Estimation between a Single-Line Scan LiDAR and a Camera

Pakapoj Tulsuk[1], Panu Srestasathiern[2], Miti Ruchanurucks[3], Teera Phatrapornnant[4] and Hiroshi Nagahashi[5]

***Abstract*— This paper presents a novel method for extrinsic parameters estimation of a single line scan LiDAR and a camera. Using a checkerboard, the calibration setup is simple and practical. Particularly, the proposed calibration method is based on resolving geometry of the checkerboard that visible to the camera and the LiDAR. The calibration setup geometry is described by planes, lines and points. Our novelty is a new hypothesis of the geometry which is the orthogonal distances between LiDAR points and the line from the intersection between the checkerboard and LiDAR scan plane. To evaluate the performance of the proposed method, we compared our proposed method with the state of the art method i.e. Zhang and Pless [1]. The experimental results showed that the proposed method yielded better results.**

I. INTRODUCTION

Nowaday, there are many applications that rely on both camera and LiDAR for data acquisition. Früh and Zakhor [2] proposed a procedure for city model reconstruction using two LiDARs and a camera in the interested area. LiDARs were both mount on a vehicle horizontally and vertically. They reconstructed a city by using the correlation of LiDAR data. Douillard et al. [3] presented a method of environment representation using data from a 2D LiDAR and a camera. They used collection of images and extrinsic parameters between the camera and the LiDAR to classify each LiDAR point with respect to detected object on the image. Premebida [4] introduced a method for pedestrian detection and tracking by fusing data of image and LiDAR. Ramos et al. [5] proposed a method for close-loop outdoor SLAM. Data of LiDAR was used to locate detected features from images in world coordinate system.

In order to measure and use data correctly, the alignment between the camera and the LiDAR must be accurately estimated. Ultimately, we then reconstruct a scene with both color and depth information. However, present calibration methods are still suffering from image and depth noises. Many researchers have introduced methods for estimating extrinsic parameters between a LiDAR and a camera. Li [6] presented a method for calibrating a single line scan LiDAR and stereo vision using a triangular planar. Wasielewski [7] also worked on the same field of LiDAR-camera calibration with 3D v-shape calibration pattern which yield non-collinear 3D feature points. Kwak et al. [8] improved Wasielewski method by weighting each point according to their reliability. In other words, any point at the middle corner of the v-shape is more reliable than points at the edges. They also compared their method with previous works using the reprojection of LiDAR data on images and then evaluated the performance. Zhou and Deng [9] studied a calibration between 3D a LiDAR and a camera. The estimation is based on plane normal vectors and coplanar points. In [10], they also presented another calibration method but using different features i.e. 3D points and 3D lines which are checkerboard boarders. Huang and Barth [11] introduced a calibration method for a multi-planar LiDAR and a conventional camera. Their geometric constraint for estimation is formulated using coplanar points. Zhang and Pless [1] proposed an algorithm for estimating orientation and position of a single-line scan LiDAR and a camera using checkerboard calibration pattern. Their algorithm and experimental setup are simple and practical. The estimating cost function is the orthogonal distances from the calibration pattern to LiDAR points. Vasconcelos et al. [12] studied a minimal solution for the extrinsic parameters estimation. They considered the estimation problem as the PnP problem and performed an analysis for the minimum case.

The proposed method is similar to the work of Zhang and Pless [1]. Namely, we utilize the checkerboard as a calibration pattern because it can simply define and also practical. The contribution of this work is a novel cost function for extrinsic parameters estimation of a LiDAR and a camera. The proposed cost function is formulated as the orthogonal distances between 2D LiDAR points and a 2D line which is the intersection of LiDAR scan plane and the calibration plane. In order to detect LiDAR points which lie on the checkerboard automatically and robustly, we employ Hough transform to detect LiDAR points and RANSAC to filter out outliers. To obtain the optimal solution, non-linear optimization is performed by applying Levenberg-Marquardt algorithm.

The remaining of this paper is organized as follow: Section II explains the notation and basic geometry concepts used. We then present the proposed estimation model in Section III. Feature extraction method is discussed in Section IV. The parameters estimation method is presented in Section V. Section VI shows the experimental results on simulated and real data. The conclusion and future work are discussed in Section VII.

[1]Pakapoj Tulsuk and Miti Ruchanurucks[3] are with Faculty of Electrical Engineering, Kasetsart University, Thailand tang_900@hotmail.com and fengmtr@ku.ac.th

[2]Panu Srestasathiern with Geo-Informatics and Space Technology Development Agency, Thailand panu.sre@gmail.com

[4]Teera Phatrapornnant with National Electronics and Computer Technology Center, National Science and Technology Development Agency, Thailand teera.phatrapornnant@nectec.or.th

[5]Hiroshi Nagahashi with Department of Information Processing, Tokyo Institute of Technology, Japan longb@isl.titech.ac.jp

978-1-4799-3637-3/14/$31.00 ©2014 IEEE

II. Notation and Basic Concept

In this section, we discuss about the notation and basic concepts used in this paper. Vector is written in boldface e.g. $\mathbf{K}$ and matrix in typewriter font e.g. $\mathtt{K}$. We define $\mathbf{P} = \begin{bmatrix} x & y & z \end{bmatrix}^\top$ as a point in 3D and $\widehat{\mathbf{P}} = \begin{bmatrix} \mathbf{P}^\top & 1 \end{bmatrix}^\top$. A 2D line is represented by $\mathbf{L} = \begin{bmatrix} \alpha & \beta & \gamma \end{bmatrix}^\top$, where α, β and γ are the parameters of line equation i.e. $\alpha x + \beta y + \gamma = 0$. A plane is represented by $\pi = \begin{bmatrix} a & b & c & d \end{bmatrix}^\top$, where a, b, c and d are the parameters of plane equation i.e. $ax + by + cz + d = 0$. Superscript i indicates the coordinate system. For instance, $\mathbf{P}^i$ is the coordinate of the point $\mathbf{P}$ in i coordinate system.

Extrinsic parameters describe orientation and position of a camera with respect to a coordinate system. They are represented by rotation matrix $\mathtt{R}$ and translation vector $\mathbf{T}$, which describe orientation and position respectively. Rotation matrix is a function of three rotation angles while translation vector consists of three values t_x, t_y and t_z which are translations in X, Y and Z axes, respectively.

Homography $\mathtt{H}$ is a transformation from one coordinate system to another one. The 3D homography transformation can be represented by a 4 by 4 matrix:

$$\mathtt{H}_j^i = \begin{bmatrix} \mathtt{R}_j^i & -\mathtt{R}_j^i \mathbf{T}_{ji}^j \\ \mathbf{0}_3^\top & 1 \end{bmatrix}, \tag{1}$$

where $\mathtt{H}_j^i$ represents the transformation from j coordinate to i coordinate systems and $\mathbf{T}_{ji}^j$ is a vector in j coordinate system from the origin of j coordinate system to that of i coordinate system. As a consequence, the coordinate of point $\mathbf{P}$ in j coordinate system can be transformed to i coordinate system by $\widehat{\mathbf{P}}^i = \mathtt{H}_j^i \widehat{\mathbf{P}}^j$. Although plane transformation also uses homography, the formulation is different. That is, the plane π in j coordinate system can be transformed to i coordinate system by $\pi^i = \mathtt{H}_j^{i\,-\top} \pi^j$, where $\mathtt{H}^{-\top}$ is the inverse transpose of the homography.

III. Proposed Geometric Constraint

A calibration plane that visible to both camera and LiDAR is used for inducing the geometric constraint. We assume that there is an intersection of two planes which are checkerboard plane π_{chk} and LiDAR scan plane π_{Li}. Since both planes have the plane $z = 0$ in their coordinate systems, i.e. calibration plane coordinate system (w) and LiDAR coordinate system (l), they are represented by $\pi_{chk}^w = \pi_{Li}^l = \begin{bmatrix} 0 & 0 & 1 & 0 \end{bmatrix}^\top$.

The LiDAR observes the checkerboard plane by sampling the intersection line as a set of points. We hypothesize that if the estimation is accurate, the orthogonal distances between LiDAR points and the intersection line of the checkerboard and LiDAR scan plane should be minimized. This geometric constraint is illustrated in Figure 1. In order to formulate the constraint, the checkerboard plane is firstly transformed from its coordinate system to camera coordinate system (c): $\pi_{chk}^c = \mathtt{H}_w^{c\,-\top} \pi_{chk}^w$. As a result,

$$\pi_{chk}^c = \begin{bmatrix} \mathbf{r}_{w(3)}^c \\ t_{wc(3)}^w \end{bmatrix}, \tag{2}$$

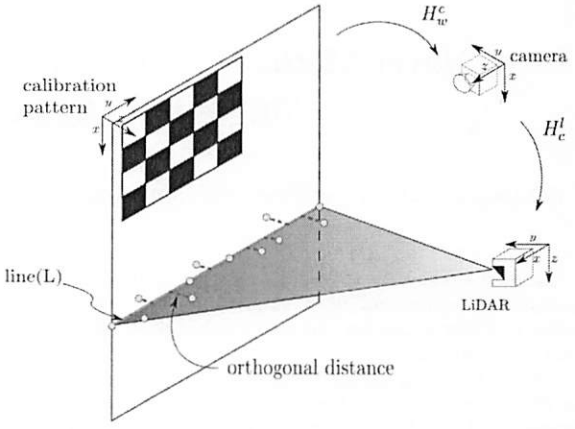

Fig. 1. The calibration setup. The calibration plane π_{chk} is red plane, LiDAR plane π_{Li} blue plane, the intersected line $\mathbf{L}$ green line and noisy LiDAR points yellow points which are generated from sampling the trace. The cost function is orthogonal distances of LiDAR points to the line $\mathbf{L}$, which are pink dash lines.

where $\mathbf{r}_{w(3)}^c$ is the third column of rotation matrix $\mathtt{R}_w^c$ and $t_{wc(3)}^w$ the third member of translation vector $\mathbf{T}_w^c$. Then transformed the checkerboard plane from camera coordinate system to LiDAR coordinate system by $\pi_{chk}^l = \mathtt{H}_c^{l\,-\top} \pi_{chk}^c$. Note that $\mathtt{R}_c^l$ and $\mathbf{T}_{cl}^c$ are estimated. Since LiDAR scan plane π_{Li}^l is the plane $z = 0$, the intersection line $\mathbf{L}^l$, which is the intersection between plane π_{chk}^l and π_{Li}^l, can be formulated by removing the third term of π_{chk}^l. Compactly, the line $\mathbf{L}^l$ is then written as:

$$\mathbf{L}^l = \pi_{Li}^l \cap \pi_{chk}^l = \mathtt{D}_1 \mathtt{H}_c^{l\,-\top} \begin{bmatrix} \mathbf{r}_{w(3)}^c \\ t_{wc(3)}^w \end{bmatrix}, \tag{3}$$

where

$$\mathtt{D}_1 = \begin{bmatrix} 1 & 0 & 0 & 0 \\ 0 & 1 & 0 & 0 \\ 0 & 0 & 0 & 1 \end{bmatrix}. \tag{4}$$

Since the LiDAR scan plane is plane $z = 0$, we represent a laser point by $\mathbf{p}^l = \begin{bmatrix} x & y \end{bmatrix}^\top$ and define $\widehat{\mathbf{p}} = \begin{bmatrix} \mathbf{p}^\top & 1 \end{bmatrix}^\top$. In the ideal case, where no noise is present, the orthogonal distance of each scanned point to the intersection line $\mathbf{L}^l$ should be zero. As a result, the geometric constraint is then:

$$0 = \frac{\widehat{\mathbf{p}}^{l\top} \mathbf{L}^l}{\| \mathtt{D}_2 \mathbf{L}^l \|}, \tag{5}$$

where

$$\mathtt{D}_2 = \begin{bmatrix} 1 & 0 & 0 \\ 0 & 1 & 0 \end{bmatrix}. \tag{6}$$

Therefore, (5) is used as the estimation model in this paper.

IV. Feature Extraction

The calibration process requires co-features which is the calibration plane that visible on both camera and LiDAR. We employ the checkerboard as a calibration pattern. The checkerboard can be automatically detected in the image

using image processing technique. However, the automatic detection of the checkerboard in LiDAR data is also required in order to make the fully automated feature detection. As a result, we suggest Hough transform and RANSAC, which provide line segment localization and outlier removal respectively.

As it is already discussed, The LiDAR observes the checkerboard as a line because of the intersection between the checkerboard and the LiDAR scan plane. The checkerboard is placed as the closest object to the LiDAR. Therefore, the checkerboard can be detected by locating the closest line to the origin in LiDAR coordinate system.

A. Hough Transform

Hough transform is the most suitable method to locate lines [13]. The concept is to transform every point in x-y space into parameter space. In order to detect lines, we define the parameter space as ρ and θ according to line equation $\rho = x\cos(\theta) + y\sin(\theta)$. After transform every point into the parameter space, local peaks in the parameter space that correspond to line candidates in x-y space can be noticed.

The closest line, the checkerboard, is defined by the minimum distance from the center of line segment to the origin. In practical, corresponding points of the line segment might contain false detection from other line segments especially when the calibration is performed indoor. In this paper, we remove the false detection using graph cut algorithm. That is, the points that are not in the densest point cluster are removed.

B. RANSAC

RANSAC is an iterative method to estimate parameters of a mathematical model, and remove outliers with respect to the model. Inliers are the majority of data that fit to the model, whereas outliers do not. Those outliers are from the confusion of the closest object cause by imperfections of experimental setup, such as the LiDAR scan on the hand of checkerboard holder. Moreover, due to the coarse step size in Hough parameter space, the obtained points possibly have outliers. Therefore, we use RANSAC to remove all the outliers.

V. Parameter Estimation

Since LiDAR data is prone to noise, in practice, the derived parameters cannot satisfy (5). Both an optimal solution and a subsequent non-linear solution are applied. The optimal solution can be obtained by solving (5) in least-square sense. That is, we hypothesize that the optimal solution minimizes (5). In order to solve the least-square problem, we firstly solve for the initial guess for the iterative process by relaxing the non-linearity of the (5). The obtained initial guess is then passed to an iterative process called Levenberg-Marquardt algorithm in order to refine the initial guess.

A. Linear Least-Square

Removing the denominator from (5), then obtained linear cost function:

$$0 = \widehat{\mathbf{p}}^{l\mathsf{T}} \mathrm{D}_1 \mathrm{H}_c^l \pi_{chk}^c, \tag{7}$$

where

$$\mathrm{H}_c^{l\,-\mathsf{T}} = \left[\begin{array}{c|c} \mathrm{R}_c^{l\,\mathsf{T}} & \mathbf{0}_3 \\ \hline \mathbf{T}_{cl}^{c\,\mathsf{T}} & 1 \end{array}\right]. \tag{8}$$

By apply vec operator to (7), we obtain:

$$0 = \left((\pi_{chk}^c)^{\mathsf{T}} \otimes (\widehat{\mathbf{p}}^l \mathrm{D}_1)\right) vec(\mathrm{H}_c^l), \tag{9}$$

where $\otimes$ is Kronecker product operator. After some algebraic manipulation, the linear least-square for estimating extrinsic parameters is obtained:

$$\mathrm{A} = \mathrm{B} vec([\mathrm{R}_c^l | \mathbf{T}_{cl}^c]), \tag{10}$$

where $vec([\mathrm{R}_c^l | \mathbf{T}_{cl}^c]) = \begin{bmatrix} r_{11} & r_{21} & r_{31} & \cdots & t_x & t_y & t_z \end{bmatrix}^{\mathsf{T}}$.

The obtained rotation matrix may not satisfy rotation matrix properties which are $(\mathrm{R}_c^l)^{\mathsf{T}} = (\mathrm{R}_c^l)^{-1}$ and $det(\mathrm{R}_c^l) = 1$. To obtain the valid rotation matrix that satisfies the aforementioned properties, the Singular Value Decomposition(SVD), $\mathrm{R}_c^l = \mathrm{UDV}^{\mathsf{T}}$, and constraint $\mathrm{R}_c^l = \mathrm{USV}^{\mathsf{T}}$, where $\mathrm{S} = diag(1, 1, det(\mathrm{U})det(\mathrm{V}))$ are used to resolve the conditions of rotation matrix according to [14].

B. Non-Linear Optimization

Normally, non-linear optimization requires an initial guess, which is from Subsection V-A. In other words, the initial solution is refined by non-linear least-square. The translation is simply parameterized by vector without imposing any constraint. Unfortunately, the properties of rotation matrix need to be imposed as constraints in the estimation model in order to obtain the correct rotation matrix. To waive the rotation matrix constraints, Triggs [15] mentioned that rotation matrix should be parameterized using local perturbation $\mathrm{R} = \mathrm{R}_0 \delta\mathrm{R}$, where R_0 is the original rotation matrix's state, $\delta\mathrm{R} = exp(\begin{bmatrix}\omega & \phi & \kappa\end{bmatrix}^{\mathsf{T}}_{\times})$ the state update and $\begin{bmatrix}\omega & \phi & \kappa\end{bmatrix}^{\mathsf{T}}_{\times}$ a skew matrix of three rotation angles. Particularly, the rotation matrix is approximated about zero rotation angle $\omega = \phi = \kappa = 0$ to locate the optimum point around the original location. Additionally, we use Levenberg-Marquardt to increase iteration speed.

VI. Results

We compare our proposed method with that of Zhang and Pless [1] using simulated and real data. In the experiment with simulated data, the comparison is performed using displacement of derived rotation matrix and translation vector to their ground truth. The estimated parameters are illustrated in terms of image with reprojected data, in the experiment using real data.

A. Simulated data

Simulated data provides us series of scenarios with controlled environment to study effects of noise to the estimation models. To measure the estimation errors, the estimated parameters are then compared with the ground truth. We established a simulation of our experimental setup to analyze the estimated parameter errors of the proposed method and that of Zhang and Pless method [1].

Given the checkerboard size and extrinsic parameters between the camera and the LiDAR, a set of LiDAR points was generated by varying the pose of camera to checkerboard. The checkerboard size is 500×700 square millimeters. The LiDAR scans along the checkerboard with 0.5 degrees angular resolution without laser light scattering. The rotation of the camera with respect to checkerboard coordinate system are randomly generated such that orthonormal property of rotation matrix is satisfied while the distance from the camera to the checkerboard limited to 2500 millimeters.

To compare the estimated parameters, i.e. rotation matrix and translation vector, with the ground truth, Riemanian and Euclidien distance respectively are used. Euclidien distance is a straightforward evaluation method to measure the displacement of position. Hence, it is applied to measure the error of estimated translation vector compared to ground truth. Let estimated translation vector be $\mathbf{T}_{est}$ and the ground truth translation vector $\mathbf{T}_{\text{ground truth}}$. Then the translation vector estimation error can be calculated by: $d_{\mathrm{T}}(\mathbf{T}_{est}, \mathbf{T}_{\text{ground truth}}) = \|\mathbf{T}_{\text{ground truth}} - \mathbf{T}_{est}\|_2$. Riemanian distance is used to measure the distance between two rotation matrices. Riemanian distance between estimated rotation matrix R_{est} and the ground truth rotation matrix $\mathrm{R}_{\text{ground truth}}$ can be calculated by:

$$d_{\mathrm{R}}(\mathrm{R}_{est}, \mathrm{R}_{\text{ground truth}}) = \frac{1}{\sqrt{2}}\|Log(\mathrm{R}_{est}^{\top}\mathrm{R}_{\text{ground truth}})\|_F, \quad (11)$$

where $\|\cdot\|_F$ is Frobenius norm. The logarithm of orthonormal matrix is:

$$Log(\mathrm{R}) = \begin{cases} 0 & \text{if } \theta = 0 \\ \frac{\theta}{2\sin\theta}(\mathrm{R} - \mathrm{R}^{\top}) & \text{if } \theta \neq 0 \end{cases}, \quad (12)$$

where θ must satisfy the conditions $trace(\mathrm{R}) = 1 + 2\cos\theta$ and $|\theta| < \pi$ (this formula breaks down when $\theta = \pm\pi$) according to [14].

The simulation is repeated 100 times with random process of additive Gaussian noise on LiDAR data. The estimation errors are obtained by averaging all trails. Figure 2 and Figure 3 illustrate the estimation errors with respect to noise standard deviation and the number of poses respectively. In the first experiment, we used 28 poses of camera to checkerboard, and varied noise standard deviation from 0-15 millimeters. Performance with respect to noise standard deviation is presented by the displacement of rotation matrix and translation vector to the ground truth, which are shown in Figure 2(a) and Figure 2(b). They show that the estimation errors from linear estimation grow rapidly with respect to noise standard deviations. In contrast, the errors from non-linear estimation grow linearly. The proposed algorithm outperforms Zhang and Pless method [1] in both linear and non-linear estimation. Performance with respect to the number of camera to checkerboard poses is presented in Figure 3(a) and Figure 3(b). In this experiment, noise standard deviation is six millimeters and the number of camera poses varied from 6-28 poses. The estimation errors reduce drastically when the number of poses increases. In other words, the higher number of poses have, the better estimation result is.

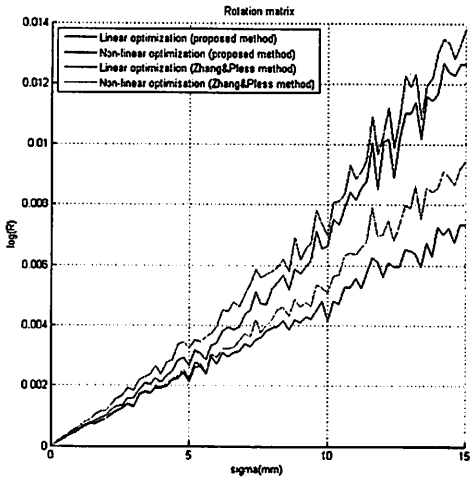

(a) Rotation matrix estimation error vs. noise standard deviation

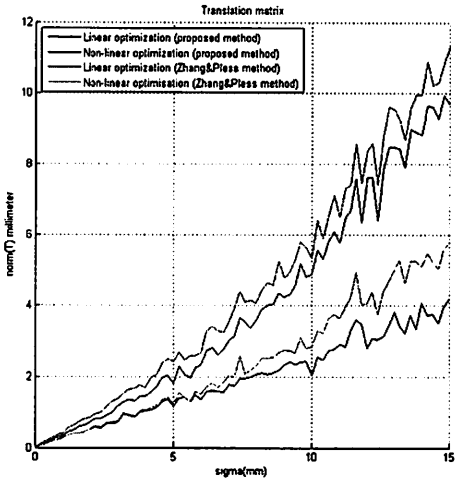

(b) Translation vector estimation error vs. noise standard deviation

Fig. 2. Rotation matrix and translation vector estimation error versus noise standard deviation. The estimation errors were measure with respect to ground truth. The proposed method is compared with Zhang and Pless algorithm in simulated scenarios.

B. Real Data

The proposed method was tested using a computer webcam camera, a modified IR webcam camera (only for

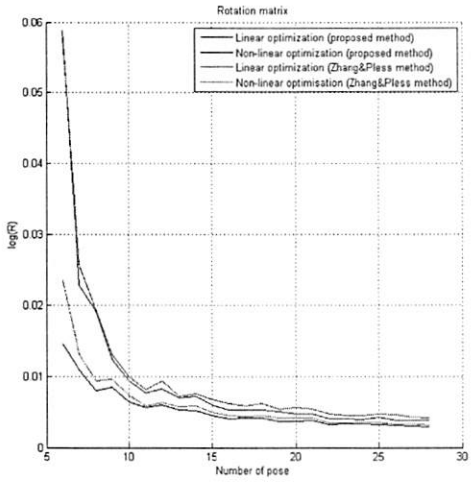

(a) Rotation matrix estimation error vs. number of poses

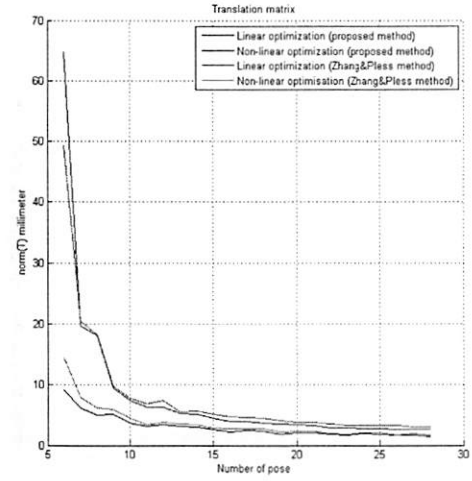

(b) Translation vector estimation error vs. number of poses

Fig. 3. Rotation matrix and translation vector estimation error versus the number of checkerboard poses. The estimation errors were measure with respect to ground truth. The proposed method is compared with Zhang and Pless algorithm in simulated scenarios.

observation) and SICK LMS 511(LiDAR). All devices were mounted on a fixed plate. Then they capture various poses of checkerboard such that the calibration plane is visible to both camera and LiDAR. Its scanning angle is between -5 to 185 degrees with 0.5 degrees angular resolution. Standard deviation on measurement range is 7 millimeters for less than 10 meters operation range. Color camera resolution is set as 1024×768. The calibration pattern consists of 7 squares × 9 squares and the size of each square is 57×57 square millimeters. The camera and the LiDAR observed the checkerboard simultaneously. We acquired more than 20 images and LiDAR scans for estimating the pose between the camera and the LiDAR. Moreover, those images are used

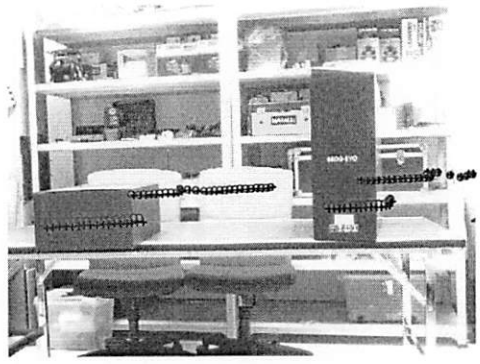

(a) Reprojected LiDAR points onto image using linear optimization

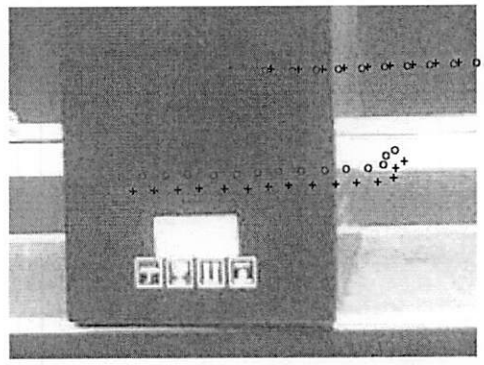

(b) Close-up of reprojected LiDAR points onto image using linear optimization

Fig. 4. LiDAR data reprojection using parameters from linear optimization. The results from the proposed method and Zhang and Pless method are presented by red circle and blue cross respectively.

for the camera calibration as well in order to obtain R_w^c and $\mathbf{T}_w^c$. The feature points, the set of points that lies on the checkerboard, are automatically picked by feature extraction process mentioned in Section IV.

The results from real data show that our proposed method is well performed and yield reliable calibration parameters. Figure 4 and Figure 5 show projected LiDAR data on the images using the parameters from linear and non-linear estimation. It can be observed that the reprojected points using the parameters from linear estimation do not match with the corner of the black box as shown in Figure 4(b). Then after non-linear optimization as shown in Figure 5(b), the reprojected points match with the corner of black box.

VII. Conclusion

This paper proposes a novel estimation model for estimating extrinsic parameters between a camera and a single line scan LiDAR which is practical, and can be applied on many applications. We constructed the geometric constraint that based on minimizing orthogonal distances of LiDAR points and the intersection line between the checkerboard

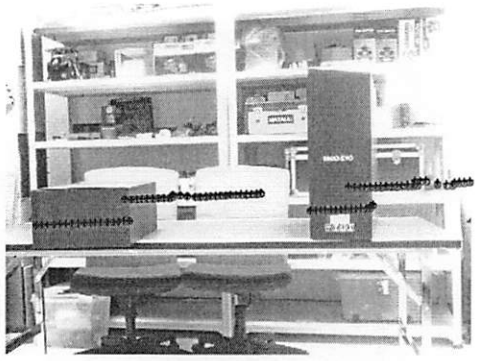

(a) Reprojected LiDAR points onto image using non-linear optimization

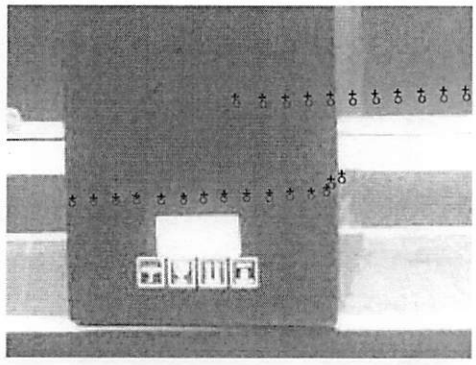

(b) Close-up of reprojected LiDAR points onto image using non-linear optimization

Fig. 5. LiDAR data reprojection using parameters from non-linear optimization. The results from the proposed method and Zhang and Pless method are presented by red circle and blue cross respectively.

and scanning plane.

Both linear least-square and non-linear optimization methods yield more sufficient efficiency. Thus, they show that our proposed model outperforms that of Zhang and Pless model. We proposed the constraint without loss of information; that is the reason that ours is superior. Moreover, our plane transformation reduces uncertainties of their point transformation Our optimization step leads to the appropriate answer because we included orthonormal property of rotation matrix to the procedure. Like many methods, the efficiency of algorithm depends on the number of checkerboard poses that is visible to the camera and the LiDAR.

In the future, we attempt to calibrate a more advance version of LiDAR such as multi-planar LiDAR or velodyne LiDAR which has more hardware complexity by applying the basic of plane transformation and homography.

ACKNOWLEDGMENT

The authors would like to thank Geo-Informatics and Space Technology Development Agency (Public Organization) who provided LiDARs SICK LMS 511. This research is financially supported by Thailand Advanced Institute of Science and Technology (TAIST), National Science and Technology Development Agency (NSTDA), Tokyo Institute of Technology and Kasetsart University (KU) under the TAIST Tokyo Tech Program.

REFERENCES

[1] Q. Zhang and R. Pless, "Extrinsic calibration of a camera and laser range finder (improves camera calibration)," in *Intelligent Robots and Systems, 2004. (IROS 2004). Proceedings. 2004 IEEE/RSJ International Conference on*, vol. 3, 2004, pp. 2301–2306 vol.3.

[2] C. Früh and A. Zakhor, "An automated method for large-scale, ground-based city model acquisition," *International Journal of Computer Vision*, vol. 60, pp. 5–24, 2004.

[3] B. Douillard, D. Fox, and F. Ramos, "Laser and vision based outdoor object mapping." in *Robotics: Science and Systems*, O. Brock, J. Trinkle, and F. Ramos, Eds. The MIT Press, 2008. [Online]. Available: http://dblp.uni-trier.de/db/conf/rss/rss2008.html#DouillardFR08

[4] C. Premebida, G. Monteiro, U. Nunes, and P. Peixoto, "A lidar and vision-based approach for pedestrian and vehicle detection and tracking," in *Intelligent Transportation Systems Conference, 2007. ITSC 2007. IEEE*, 2007, pp. 1044–1049.

[5] F. Ramos, J. Nieto, and H. Durrant-Whyte, "Recognising and modelling landmarks to close loops in outdoor slam," in *Robotics and Automation, 2007 IEEE International Conference on*, 2007, pp. 2036–2041.

[6] G. Li, Y. Liu, L. Dong, X. Cai, and D. Zhou, "An algorithm for extrinsic parameters calibration of a camera and a laser range finder using line features," in *Intelligent Robots and Systems, 2007. IROS 2007. IEEE/RSJ International Conference on*, 2007, pp. 3854–3859.

[7] S. Wasielewski and O. Strauss, "Calibration of a multi-sensor system laser rangefinder/camera," in *Intelligent Vehicles '95 Symposium., Proceedings of the*, 1995, pp. 472–477.

[8] K. Kwak, D. Huber, H. Badino, and T. Kanade, "Extrinsic calibration of a single line scanning lidar and a camera," in *Intelligent Robots and Systems (IROS), 2011 IEEE/RSJ International Conference on*, 2011, pp. 3283–3289.

[9] L. Zhou and Z. Deng, "Extrinsic calibration of a camera and a lidar based on decoupling the rotation from the translation," in *Intelligent Vehicles Symposium (IV), 2012 IEEE*, 2012, pp. 642–648.

[10] ——, "A new algorithm for computing the projection matrix between a lidar and a camera based on line correspondences," in *Ultra Modern Telecommunications and Control Systems and Workshops (ICUMT), 2012 4th International Congress on*, 2012, pp. 436–441.

[11] L. Huang and M. Barth, "A novel multi-planar lidar and computer vision calibration procedure using 2d patterns for automated navigation," in *Intelligent Vehicles Symposium, 2009 IEEE*, 2009, pp. 117–122.

[12] F. Vasconcelos, J. Barreto, and U. Nunes, "A minimal solution for the extrinsic calibration of a camera and a laser-rangefinder," *Pattern Analysis and Machine Intelligence, IEEE Transactions on*, vol. 34, no. 11, pp. 2097–2107, 2012.

[13] W. Burger and M. J. Burge, *Principles of Digital Image Processing. Core Algorithms*. Springer-Verlag London Limited, 2009.

[14] M. Moakher, "Means and averaging in the group of rotations," 2002.

[15] B. Triggs, P. Mclauchlan, R. Hartley, and A. Fitzgibbon, "Bundle adjustment a modern synthesis," in *Vision Algorithms: Theory and Practice, LNCS*. Springer Verlag, 2000, pp. 298–375.

TECHNICAL PROGRAM

Monday, June 16

13:30-14:50, San pa Tong Room

A1: Spatio-temporal statistics and analysis for moving objects

086
Geospatial Analysis of Poverty Incidence in Pasay City, Philippines using Ordinary Least Squares and Geographically Weighted Regression
Ariel C. Blanco

101
Spatial and Temporal Variations of PM2.5 in China
Yulian Yang

052
Spatial Fishing Migration Patterns of Squid Fishermen at Salura Island Indonesia
Dewi Susiloningtyas

058
3D Reconstruction of Canal Profiles Using Data Acquired from Teleoperated Boat
Supannee Tanathong

13.30-14.50, San Pa Tueng Room

A2: Geo-big data management and mining

003
Data Management for Large-Scale Trajectory Data Analysis using Hadoop/Hive with Spatial Enablement
Apichon Witayangkurn

032
A Pattern Matching Method for Extracting Road Traffic Information from Web Texts
Peiyuan Qiu

039
Domain vocabulary generated by academic paper database in geographic information science
Masafumi Ono

094
Integrating 3D Space-Time Visualisation with Online Analytical Processing and Data Warehouse
Garavig Tanaksaranond

13:30-14:50, San Pa Liang Room

A3: Laser scanning and UAV/Location based services (LBS)

011
Utilizing GIS Data In A Modeling And Simulation Tool For UAV Mission Planning
Nirut Chalainanont

060
LiDAR height transformation with Geoid surface modeling using interpolation method in Bangkok metropolitan area
Worapod Masiri

076
Complex Building Model Generation through Integrating LiDAR and Aerial Photos
Ruifang ZHAI

020
DEVELOPMENT OF KARACHI GIS USING LOCATION BASED SERVICES (LBS)
Aamir Ali

036
An improved index mechanism for efficient POI search in Location Based Service
Zhan-Ya Xu

15:10-16:50, San pa Tong Room

B1: GIS for Environmental Resources & Management

022
Analysis of Spatio-Temporal for Flood Inundation Area Using MODIS Images For Chao Phraya River Basin of Thailand
Hyung-Jin Shin

031
Public Participation Spatial Decision Support System For Integrated Watershed Management
Rong-Kang Shang

041
Mapping Groundwater Potential Zones using Analytic Hierarchy Process (AHP) in Banteay Meanchey Province, Cambodia
Sainglong Kaing

068
IMPROVING IRRIGATION MONITORING SOFTWARE WITH GEOGRAPHIC INFORMATION
Phagasinee Boottho

077
BASIN WATER ENVIRONMENTAL EFFECTS OF URBAN LANDSCAPE
Wang Guilin

Monday, June 16

15:10-16:50, San Pa Tueng Room

B2: GeoComputation

055
Building Community Networks for Preserving Local Resources with Web-based GIS
Sally E. Goldin

057
Texture Based Classification of High Resolution Remotely Sensed Imagery Using Weber Local Descriptor
Decky Aspandi Latif

004
Development of Geo-portal For Precise Farming In Saraburi, Thailand
Ashik Rajbhnadari

009
AN APPROACH OF GEO-COMPUTATION FOR AUTOMATIC PLACEMENT OF 3D BUILDING MODELS
Nirut Chalainanont

010
Spatial Knowledge Criteria Extraction from Urban Building's Regulations in Bangkok
Chomchanok Liangwannaphorn

069
The investigation of viewing angle effects on ground sampling distance of Thaichote satellite imagery
Sittipun Sangsuwan

15:10-16:50, San Pa Liang Room

B3: GIS for Environmental Resources & Management

019
FRAMEWORK DESIGNING OF A HEALTH - GISYSTEM FOR TELE-EPIDEMIOLOGICAL ANALYSIS OF INFECTIOUS DISEASES
Daniyal

056
A Slope Stability Assessment in the Tropics
Emba Tampang Allo

061
Development of GIS Database for Conservation and Sustainable Use of Lampradong: A Case Study of Amphawa District, Thailand
Farida Duriyapong

087
SPATIAL ANALYSIS OF DROUGHT AREA IN KHUAN KHRENG WETLAND USING GEO-INFORMATICS TECHNOLOGY : METHODOLOGY DESIGN
Anan Khampeera

111
Mapping and Measuring Social Vulnerabilities of Coastal areas of Bangkok and Periphery
Wijitbusaba Marome

Tuesday, June 17

9:00-10:40, Pa Sak Luang Room

C1: Real-time GIS/Location based services (LBS)/GIS for geo-spatial services/ GIS for Environmental Resources & Management

007
Towards Live Virtual Geographic Environment
CHE Weitao

023
Development of the Standard Data Model for Interoperability of the River GeoSpatial Data
Hyo-Sok Chae

078
The Design And Implementation Of GIS Combined with Baidu Map Application System Contruction
Wang Guilin

002
The Assessment of spatial distribution and allocation of nursery schools using GIS with Social justice approach (A case study Zanjan city)
Mohsen Ahadnejad Reveshty

067
Development of a Geo-Spatial Thinking Ability Test
Jinn-Guey Lay

9:00-10:40, San Pa Tong Room

C2: GIS for Environmental Resources & Management

005
Land Suitability and Crop Substitution Modeling for Sugarcane and Cassava in Thailand
Tamkuan Nopphawan

013
Crop Yield Estimation: Integrating RS, GIS and Field Measurement for supporting smart farm project in Huaykhamin, Saraburi,Thailand
Kulapramote Prathumchai

074
Assessment of Economics Crops Damaged in Flooded Area: An Implemented on Chalerm Phra Kiat District, Pak Phanang Sub-Watershed, Thailand
Tussana Pol-on

042
Tree Plantation Area Detection Corresponding to Employment
Creations in Central Laos Using Satellite Remote Sensing
Satomi Kimijima

066
Monitoring of Coastal Dynamic Sand Dunes Parangtritis Using Remote Sensing and GIS
Annacletus Ari Dartoyo

Tuesday, June 17

11.00-12.20, Pa Sak Luang Room

D1: GIS for transportation applications

006
GPS Enabled Taxi Probe's Big Data Processing For Traffic Evaluation Of Bangkok Using Apache Hadoop Distributed System
Saurav Ranjit

054
Potential For Fire Emergency Response System In Urban Area Base On GIS Technology
Thoa Nguyen

048
The Analysis and Inspiration from Monalisa Maritime Project of EU
Peng Guojun

100
Estimate Highway Traffic Demand using Large Scale Mobile GPS: A Case Study of Japan Highway Networks
Teerayut Horanont

044
Ground Deposition Mapping of 137Cs Discharged from Fukushima Daiichi Nuclear Power Plant
Nobuhiro Sawano

11.00-12.20, San Pa Tong Room

D2: GIS for Environmental Resources & Management

037
Analysis on Rainfall and Dry spell Probability and Change in Decade for the Upper North of Thailand
Wilasluk Wongwai

093
URBAN GROWTH USING REMOTE SENSING AND SPATIAL METRICS
Suwannee Wutthiwong

123
From Social media information to VGI: mining data from Weibo when in an emergency
Chao Yang

133
Hierarchial Polygonization Method in Automatic GIS-T Information Generation and Updating from Road Marking Database
Anthony G.O. Yeh

136
Groundwater Exploration Using Fuzzy Logic Approach in GIS, Area around an Anticline, Fars Province, Iran
Rafati, S